AIAA 80-0271R

Supersonic Inviscid Flowfield Computations of Missile Type Bodies

A. B. Wardlaw Jr.,* J. M. Solomon,† and F. P. Baltakis‡
Naval Surface Weapons Center, Silver Spring, Md.

A finite-difference method suitable for design calculations of finned bodies is described. Efficient numerical calculations are achieved using a thin fin approximation that neglects fin thickness but retains a correct description of the fin surface slope. The resulting algorithm is suitable for treating relatively thin, straight fins with sharp edges. Methods for treating the fin leading and trailing edges are described that are dependent on the Mach number of the flow normal to the edge. The computed surface pressures are compared to experimental measurements taken on cruciform configurations with supersonic leading and trailing edges and to a swept wing body with detached leading-edge shocks. A semiempirical procedure is developed to treat the leading edges in the latter case. Measured and calculated pressures are in reasonable agreement in both the tested configurations.

I. Introduction

A PRACTICABLE means of predicting the nonlinear, inviscid, supersonic shock layer on missile configurations is to numerically solve the steady, three-dimensional inviscid equations using an efficient finite-difference method. Several computer programs are currently available for this purpose, e.g., Refs. 1-7. Although these supersonic flowfield codes can be applied to relatively arbitrary body shapes, their application to practical wing-body-tail configurations presents some serious computational problems. Existing codes treat the complete fin-body cross section as a single entity. Thus when cylindrical coordinates, as shown in Fig. 1, are used a large number of ϕ mesh planes are needed to resolve the fin adequately. When several fins are present at the same axial station, the number of grid points needed becomes prohibitively large for practical design calculations. The number of grid points can be reduced substantially by mapping the fin body cross section into a more "rounded" figure. The existing methods of utilizing this approach are based on conformal mapping techniques developed by Moretti[2,8] (see also Refs. 3 and 6). The mappings, however, are complicated even for the case of a single smooth fin or wing and often tend to cluster large numbers of mesh points near wing tips. This reduces the permissible marching step and increases computational time. Fin surface geometries often considered consist of segmented surfaces with sharp corners and edges. The flow on and downstream of the fin surfaces is dominated by expansions and/or shocks emanating from these edges and corners. These discontinuities must be approximated accurately within the confines of the rather coarse computational grid dictated by practical design calculations.

The primary focus of the present study is the development of a more efficient numerical technique for treating finned bodies. To achieve this, the approach used here departs from the basic computational strategy used in Refs. 1-7 when fin surfaces are present. Instead of considering the cross-sectional body-fin geometry as a single entity, the present approach considers the body alone (i.e., the body with all fin surfaces removed) and the fin geometry separately. The computational grid is generated using normalizing transformations[1,4,5,7] applied to the body-alone configuration. The fin surfaces are allowed to extend into the computational region and can be resolved adequately within a relatively coarse computational grid. In order to treat the complex flow in the immediate vicinity of fin leading and trailing edges, appropriate local analyses are built into the program which depend strongly on the local Mach number of the flow component normal to the edge. These local analyses can range from locally exact, when the edge is sharp and the normal velocity component is sufficiently supersonic, to ad hoc or semiempirical in other situations.

Within this framework, various approaches for numerically treating general fin surface shapes are possible. One approach would be to introduce extra computational points to represent the fin surfaces which would float within the basic grid. This would complicate the application of the boundary conditions on the fin surfaces. Another approach, which would eliminate this difficulty, would be to subdivide the flow domain into several subregions each containing the flow between adjacent fin surfaces. Relatively simple transformations would be applied separately in each subregion to map adjacent fin surfaces onto constant computational coordinate planes. Relatively coarse meshes could be used in each subregion and the computations in the various subregions could be linked in a manner suggested by Hindman et al.[9] Both the aforementioned approaches are in principle capable of handling general fin surface geometries.

To simplify the development for the present study, the analysis is restricted to relatively thin fins with sharp edges which lie approximately along constant ϕ planes (cf., Fig. 1). A thin fin approximation is employed that neglects the fin thickness but retains the actual fin surface slopes. For an important class of body-fin configurations, the thin fin approximation allows the direct use of the basic grid generated for the body-alone shape (see Sec. II) without the introduction of floating points to describe the fin surface or additional mappings. To verify the thin fin approximation and the associated computational method presented here (see Secs. II and III), comparisons are made of computed and measured surface pressure distributions for several fin-body configurations. A representative sampling of these is presented in Sec. IV.

II. Notation and Preliminaries

The numerical methods for treating fin-body combinations presented here differ from existing supersonic inviscid flowfield codes[1-7] only in the treatment of fin surfaces. In the present work, the procedures for treating fin surfaces, which appear in Sec. III, will be described and implemented within

Presented as Paper 80-0271 at the AIAA 18th Aerospace Sciences Meeting, Pasadena, Calif., Jan. 14-16, 1980; submitted Jan. 28, 1980; revision received Jan. 27, 1981. This paper is declared a work of the U.S. Government and therefore is in the public domain.

*Aerospace Engineer, Applied Mathematics Branch. Member AIAA.
†Mathematician, Applied Mathematics Branch. Member AIAA.
‡Aerospace Engineer, Aerodynamics Branch. Member AIAA.

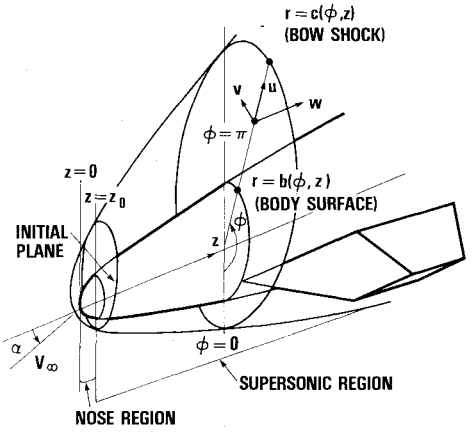

Fig. 1 Cylindrical coordinate system used for inviscid flow calculation.

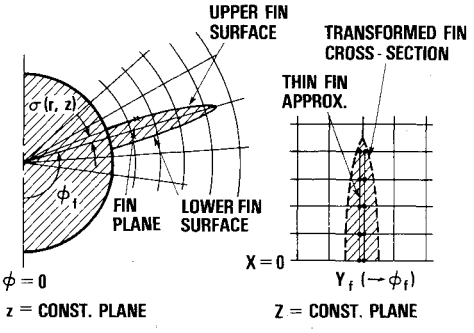

Fig. 2 Cross sectional view of the thin fin approximation.

the context of the algorithm described in Refs. 7 and 9. However, this fin treatment can be adapted in a straightforward manner to other existing supersonic inviscid flow codes that have the capability of treating internal shock waves either by "tracking" or "capturing."

A body-oriented cylindrical coordinate system (r,ϕ,z) depicted in Fig. 1 is used in this study. Standard notation will be used; viz., ρ is the density, p the pressure, h the enthalpy, a the sound speed, γ the ratio of specific heats, and q the velocity vector with components (u,v,w) as indicated in Fig. 1. It is assumed that for $z \geq z_0$, $w > a$ everywhere. For computational purposes, attention is restricted to the region $z \geq z_0$ between the body alone, expressed by $r = b(\phi,z)$ and the bow shock wave, expressed by $r = c(\phi,z)$. This region is mapped into the computational region $Z \geq z_0$, $0 \leq X \leq 1$, $0 \leq Y < 1$ by the standard normalizing transformations [1,4,5,7]

$$Z = z, \quad X = (r-b)/(c-b), \quad Y = \phi/\phi_0 \tag{1}$$

where ϕ_0 is the ϕ value of a symmetry plane, if one exists, and 2π otherwise. Every computational plane $Z = \text{const}$ is covered by a grid with uniform ΔX and ΔY. As will be described in Sec. III, the fin cross section is represented by the thin fin approximation as double valued grid points lying along portions of certain $Y = \text{const}$ grid lines; cf., Fig. 2.

The algorithm for advancing the unknown flowfield quantities from $Z = Z^k$ to the next axial station $Z = Z^k + \Delta Z$ depends on the location of the individual mesh points in the shock layer. These are divided into the following four types: interior, body surface, shock, and fin surface points. The numerical procedures used to treat the first three types of points are essentially the same as those given in Refs. 7 and 9. The only difference is that the inviscid, weak conservation equations have been recast to simplify the source term. For interior points the MacCormack predictor-corrector scheme is applied directly to the associated conservation form of these equations in the X, Y, Z space. The points on the body and bow shock surfaces are treated using predictor-corrector methods applied to certain characteristic compatibility relations for each surface along with the appropriate flow boundary conditions. See Refs. 7, 10, and 11 for complete details.

III. Computational Procedure for Fin Surfaces

Thin Fin Approximation

The thin fin approximation is applicable to fins with surfaces that lie close to a constant ϕ plane, say $\phi = \phi_f$, which is defined as the fin plane. The fin geometry is assumed to be represented by two surfaces, the upper and lower surfaces, each described independently by relations of the form

$$\phi = \phi_f + \sigma(r,z) \tag{2}$$

In the cross section $Z = \text{const}$ the actual fin surfaces will lie within the computational mesh as shown in Fig. 2. The thin fin approximation assumes that $|\sigma|$ is small, and thus places the fin surfaces along the fin plane corresponding to $Y = Y_f$ in each $Z = \text{const}$ plane. Although the fin is approximated by a zero thickness plane lying on $\phi = \phi_f$, the correct description of the fin surface slope is retained. Approximations of this type are commonly employed in slender body theory; however, in the present work no linearization of the flow equations is employed. Only the fin surface slopes and their r and z derivatives are required. The derivatives of σ, correct to $0(|\sigma|)$, are given by

$$r\sigma_r = \tan\theta, \quad r\sigma_z = \tan\nu, \quad r\sigma_{rr} = \sec^2\theta(\theta_r - \sigma_r) - \sigma_r$$

$$r\sigma_{zz} = \sec^2\nu\nu_z - \sigma_r\tan^2\nu, \quad r\sigma_{rz} = \sec^2\theta(\theta_z - \sigma_z)$$

Here θ and ν are the angles between the fin surface tangency plane and the fin plane in the r and z directions, respectively. Within the restriction that $|\sigma|$ be "small," the thin fin approximation can be applied to arbitrary fin geometries including surfaces with discontinuous slopes and fins with small deflections, camber, and variations in dihedral.

Numerical Procedure for Fin Surfaces

The numerical algorithm for treating fins by the thin fin approximation requires that the computational mesh be chosen so that each fin plane is coincident with a computational mesh plane, $Y = Y_f$. Two sets of computational points are carried on the $Y = Y_f$ plane to describe the flow properties on the upper and lower surfaces (cf., Fig. 2). As the calculation is marched down the length of the body, fin surfaces are encountered on $Y = Y_f$. Thus a point at some X may at one axial location be an interior flowfield point and in the next axial step move onto the fin. The interior point is split into two points corresponding to the upper and lower fin surfaces. The fin points thus created are referred to as leading-edge points. For a fixed X, a pair of points that are on the fin at one axial step can in the next step move off the fin and become a single interior flowfield point. Such a point will be referred to as a trailing-edge point. The flow variables at leading- and trailing-edge points are determined from an appropriate local analysis that is described in the following subsections. The adjustment for the presence of a leading or trailing edge is made immediately after the completion of the step in which the edge is encountered. The values of the flow variables prior to the adjustment are termed "upstream" while the adjusted values are termed "downstream."

All points on the fin surfaces not designated leading- or trailing-edge points are advanced using certain characteristic compatibility relations and the tangent flow boundary condition as described in Ref. 11. These relations are evaluated numerically within the framework of the thin fin approximation by placing all fin surface flow quantities on the fin plane and making all evaluations at the fin plane. The

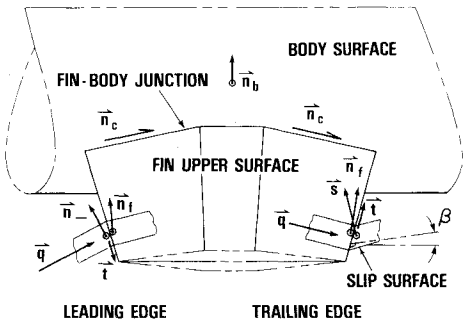

Fig. 3 Vectors used in the fin leading- and trailing-edge analysis.

juncture of the fin and the body is assumed to be a sharp corner where the flow velocity is directed along the corner. This condition and special characteristic relations[11] are used to advance the points along the juncture. Discontinuities in the fin surface slope are explicitly treated using essentially the same techniques as those for treating discontinuities in the body surface slopes given in Refs. 7 and 10 with appropriate modifications to account for the form of Eq. (2) defining the fin surface.

Leading-Edge Points

The downstream flow properties at leading-edge points are determined by a local analysis based on the computed flow upstream of the edge and the prescribed local fin geometry. The vectors used to characterize the local flow at the leading edge are shown in Fig. 3. The upper and lower surface normals at the edge n_f and the direction of the edge t are given by the fin geometry. The computed upstream velocity q and t determine the stream surface with normal $n_- = t \times q$ except in the special case where q and t are parallel. In this case, the flow automatically satisfies the boundary conditions and no additional analysis is required. The character of the flow at the leading edge is governed by the Mach number of the upstream flow component normal to the edge given by

$$M_n = \{ (n_- \times t) \cdot q \} / (|n_- \times t| a)$$

When the upstream flow crosses the leading edge with $M_n > 1$ an attached shock or expansion fan occurs in most cases that permits a local analysis (see, e.g., Chap. XI of Ref. 12). The velocity component tangent to the edge $q \cdot t$ is unaffected by the edge and all other downstream flow quantities are determined by turning the normal flow component using either an oblique shock or a Prandtl-Meyer expansion. Each surface is treated independently and the turning angle is given by

$$\delta = \cos^{-1} \{ (n_- \cdot n_f) / (|n_-| \, |n_f|) \}$$

For the upper surface, when $n_f \times n_- \cdot t < 0$ the flow is turned by an attached oblique shock and when $n_f \times n_- \cdot t > 0$ the flow is turned by a centered expansion. The same sign convention applies for the lower fin surface edge. A similar procedure for the case of an attached oblique shock has also been used in Ref. 6. In Ref. 6, the propagation of the leading-edge shocks is tracked downstream of the edge whereas in the present work these shocks are captured using the conservative and dissipative properties of the interior point scheme without additional numerical smoothing.

At leading edges where a compression turn is required, the condition $M_n > 1$ does not guarantee the existence of an attached oblique shock. For sufficiently large δ, a detached shock wave will be present and a purely local analysis is at best an approximation. However, it has been possible to formulate empirical rules for determining reasonable leading-edge conditions (see Sec. IV). When a detached shock occurs, the upper and lower fin surfaces are treated independently of one another. If one surface permits either an attached shock or a Prandtl-Meyer expansion this procedure is applied as described earlier. Such an approach is suggested by the experimental data of Ref. 13. When the upstream flow crosses the edge with $M_n < 1$, the flow at the leading edge is free of shock waves. The resulting subsonic leading-edge problem has not been investigated extensively during the current study. In the present work, the upstream normal flow component is isentropically stagnated and the resulting flow variables are assigned to both fin surfaces. At a leading edge it is possible to have $M_n < 0$ which physically corresponds to an upstream flow that does not cross the edge onto the fin surface. In the experience of the authors this situation occurs infrequently, typically at the tips of nearly rectangular fins, and always with $|M_n|$ much less than unity. This contingency is treated in the same manner as the subsonic leading edge.

For the leading-edge points at the fin-body juncture a special procedure is required. The flow in the vicinity of these points features a complicated shock interaction pattern which probably cannot be resolved within the relatively coarse mesh used in the present calculations. Accordingly, a simple heuristic procedure is used to determine the flow variables immediately downstream of the leading-edge corners. Note that the upstream velocity q on the body lies in the body tangency plane which also contains the corner direction $n_c = n_f \times n_b$ (cf., Fig. 3). The flow downstream of the leading-edge corner is obtained by rotating the velocity q within the body tangency plane and aligning it with the corner n_c, using either the oblique shock or the Prandtl-Meyer turning relations. Each surface is treated independently and the turning angle is given by

$$\delta = \cos^{-1} \{ q \cdot n_c) / (|q| \, |n_c|) \}$$

The turn is by expansion or compression on the upper surface when $n_c \times q \cdot n_b$ is positive or negative, respectively. The same sign convention applies on the lower surface.

Trailing-Edge Points

At a trailing edge the two points on $Y = Y_f$ representing the upper and lower fin surfaces are coalesced into a single interior flowfield point. A local analysis is used to determine the flow downstream of the edge from the computed flow on each fin surface upstream of the edge and the given local fin geometry. The vectors used to characterize the local flow at the trailing edge are shown in Fig. 3. Here the upper and lower surface normals n_f and the edge direction t are given by the fin geometry. The flow at the trailing edge is characterized by the Mach number of the upstream flow component normal to the edge on each surface. These are given by

$$M_n = (t \times n_f \cdot q) / (|t \times n_f| a)$$

where q is the computed velocity vector upstream of the edge on each surface.

When $M_n > 1$ for the upper surface and $M_n < -1$ for the lower surface, the upstream flow crossing the trailing edge on both surfaces is supersonic (cf., Fig. 3). In this case, either an oblique shock wave or an expansion fan occurs in most instances at the trailing edge on each fin surface. The flow leaving the fin from these surfaces is separated by a slip surface (contact discontinuity). This flowfield can be analyzed locally near the trailing edge. On each side of the fin, the tangential component of velocity $q \cdot t$ is unchanged across the trailing edge and the flow normal to t is given by a two-dimensional oblique shock or Prandtl-Meyer turning relation (see, e.g., Chap. XI of Ref. 12). A slip surface is introduced which makes an angle β with the fin plane in the plane normal to the edge as shown in Fig. 3. The components of the slip surface normal s can be obtained using the conditions $s \cdot e_3 = |s| \cos\beta$, $s \cdot t = 0$ and noting that $s \cdot e_3 = 0$ where e_3 is the unit vector in the positive ϕ direction. For a specific value of

β, the upstream flow in each surface is turned into the slip surface using an appropriate oblique shock or Prandtl-Meyer expansion. The required turning angle is given by

$$\delta = \cos^{-1}\{(\boldsymbol{s}\cdot\boldsymbol{n}_f)/(|\boldsymbol{s}|\,|\boldsymbol{n}_f|)\}$$

For the upper surface, the turn is by expansion or compression when $\boldsymbol{s}\times\boldsymbol{n}_f\cdot\boldsymbol{t}$ is negative or positive, respectively. The same sign convention applies for the lower surface. The value of β is adjusted by an iterative procedure until the pressure is the same on both sides of the slip surface. In the present work, no attempt is made to explicitly treat the resulting slip surface in the calculations downstream of the trailing edge. The flow variables at the coalesced interior point are assigned by averaging the velocity components on each side of the slip surface, using the known stagnation enthalpy to calculate h, and determining ρ from the equation of state.

As in the leading-edge case, the preceding analysis breaks down for certain combinations of low supersonic M_n and compression turning angles. This situation and all cases involving subsonic M_n or back flow at one or both trailing-edge surfaces have not been investigated extensively in the present study. These contingencies currently are treated by averaging the upstream values of p, ρ, u, and v for each surface and defining w by using the known stagnation enthalpy.

A modified treatment is used for the trailing edge occurring at the body-fin junction. Preliminary flowfield values are arrived at using the standard trailing-edge algorithm described earlier. The velocity vector is then additionally rotated within the slip plane using shock or expansion turning relations until it lies tangent to the body surface. When the iterative procedure fails to produce a converged solution, and in all other cases, the flow variables are assigned by averaging the upstream values of u, v, w, and p and using the known stagnation enthalpy and the equation of state to determine ρ.

Special Differencing Procedures

Special treatment is provided for advancing the outermost grid point on the fin surfaces, at say, $X=X_\ell$, and the adjacent interior flow point, $X_{\ell+1}=X_\ell+\Delta X$. The MacCormack scheme for advancing the interior flow point $X_{\ell+1}$ must be modified since there are two sets of flow values at X_ℓ corresponding to the upper and lower fin surfaces. The present procedure is to advance the flow variables at $X_{\ell+1}$ by the basic interior point scheme using the flow values at X_ℓ corresponding to the upper surface and then repeating the calculation at $X_{\ell+1}$ using the lower surface values at X_ℓ. The two corrector values of the conservation vector U are then averaged to obtain the final value of U at $X_{\ell+1}$. When the Mach number of the flow component normal to the edge separating X_ℓ and $X_{\ell+1}$ is supersonic, an additional modification is made to the algorithms for advancing the flow variables at both these points. Here the numerical scheme for each of these points involves X differences between X_ℓ and $X_{\ell+1}$ which are separated by a flow discontinuity originating at the edge. In the present code, there are two separate procedures for handling this difficulty. The first uses appropriate one-sided X differencing at X_ℓ and $X_{\ell+1}$, while the second simply sets the Z derivatives to zero at these points. The former has been found to produce numerical oscillations in cases involving highly swept wings and, hence, the second approach is currently favored.

Special Y-differencing procedures are also applied downstream of leading edges which feature attached shock waves. It has been found, in example calculations on two-dimensional rectangular fins, that the standard procedure for advancing the fin surface points predicts inaccurate surface pressures immediately downstream of such discontinuities. In this region, the Y differences used to advance the fin surface flow variables must be taken across the oblique shock generated by the surface discontinuity or the leading edge. These Y differences will be unrealistic for roughly the number of marching steps required for the numerical representation of the oblique shock to propagate beyond the first row of interior grid points. To circumvent this problem, an estimate is made of the number of steps required for the shock to move out to the adjacent row of points. For this number of steps, the Y differences used in the fin surface calculation are multiplied by a factor which is zero at the discontinuity and increases to unity after the estimated number of steps. This procedure is applied only after compression discontinuities have been encountered and only along the grid lines crossing the discontinuity.

IV. Numerical Results

The results computed with the present code are presented in this section and compared with the experimental data reported in Refs. 14 and 15. The investigated cases consist of pointed, axisymmetric body-wing and body-tail configurations in the Mach number range between 2.9 and 4.5 and at incidences up to 8 deg. The wing and tail surfaces have sharp leading and trailing edges which at the examined conditions feature normal velocity components that are supersonic. All computations assume a perfect gas with $\gamma=1.4$. Mesh sizes of 13×14 (i.e., $\Delta\phi=15$ deg) and 37×41

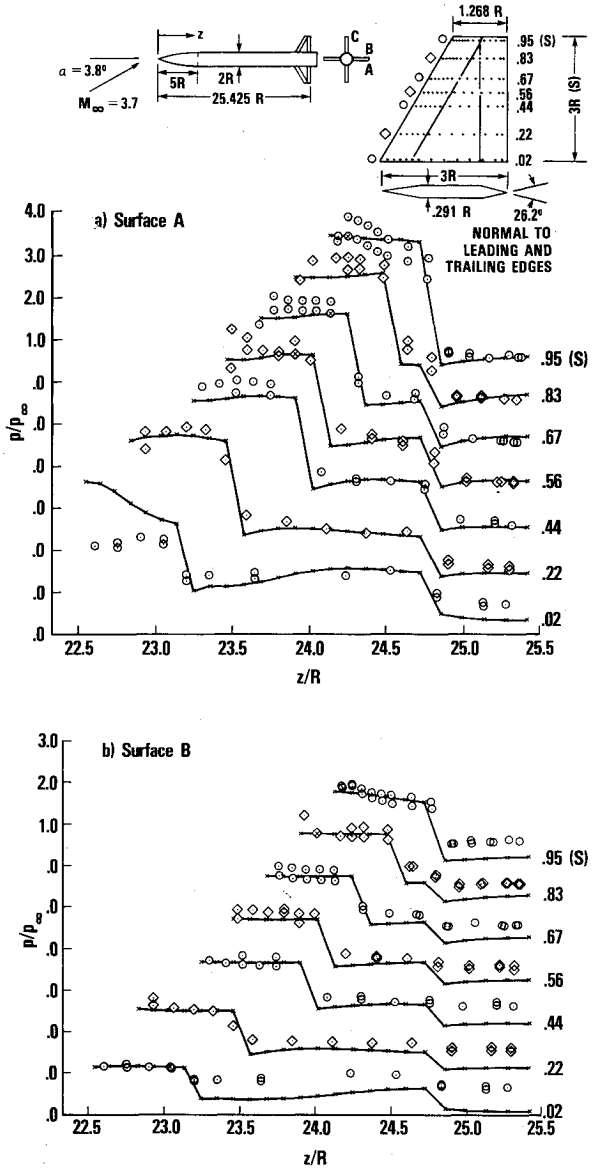

Fig. 4 Comparison of computed and measured fin surface pressures on the clipped delta fin configuration at $\alpha=3.8$ deg.

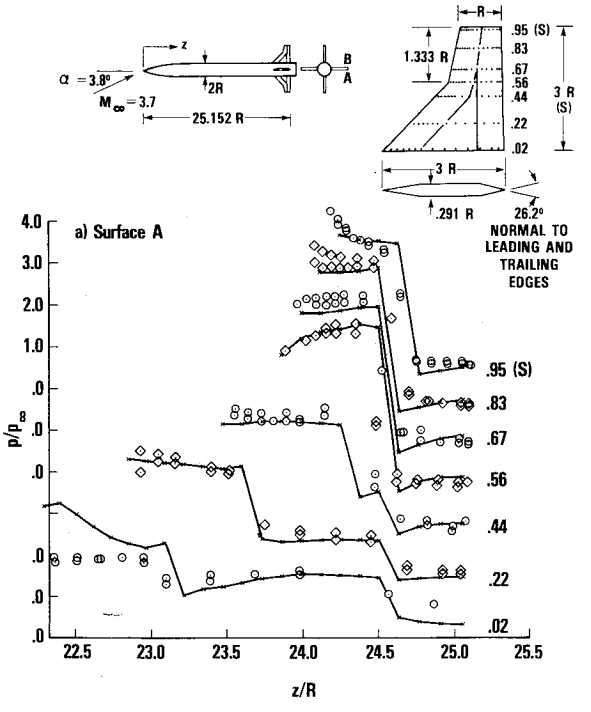

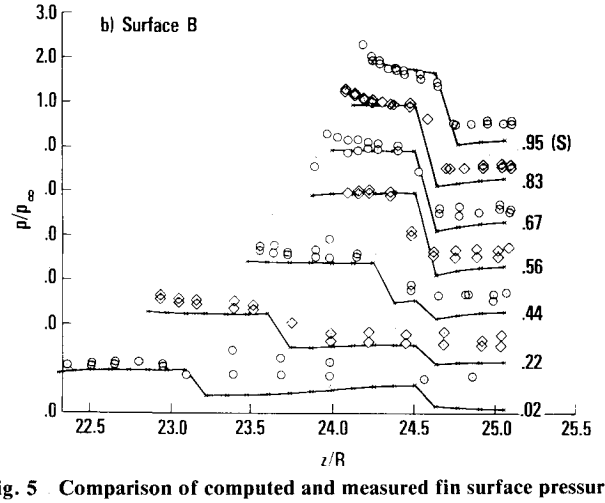

Fig. 5 Comparison of computed and measured fin surface pressures on the cranked tail configuration at $\alpha = 3.8$ deg.

(i.e., $\Delta\phi = 5$ deg) are used for the body-wing and body-tail configurations, respectively. The computations are started near the body vertex using a numerically generated conical flowfield.[11] To facilitate a comparison of numerical results with experiment, the calculated values have been interpolated to provide pressures along the same lines at which measurements were taken.

In Ref. 14 a tangent ogive body equipped with tail fins of several different planforms is tested in supersonic flow. Numerical results are compared to experimentally measured surface pressures taken at Mach 3.7 for configurations featuring clipped delta and cranked tail fins. The data was taken at a freestream Reynolds number (based on diameter) of 1.8×10^5. Both types of fins feature surface slope discontinuities at various locations along the surface. The freestream Mach number is sufficiently large to allow an attached shock solution at the fin leading edge except on the cranked tail at an incidence of 8 deg. Here body upwash creates a large angle of attack in the immediate vicinity of the body and the shock is predicted to be detached locally. The leading-edge pressure, density, and velocity are assigned using the algorithm outlined later in this section.

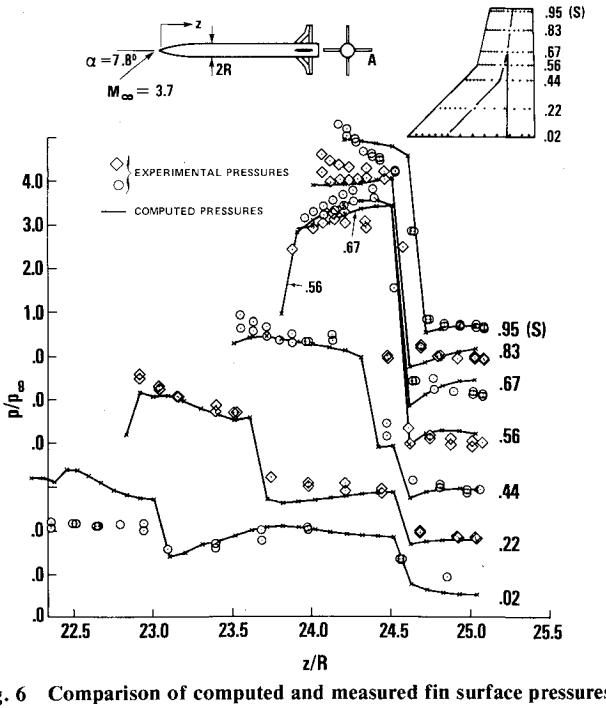

Fig. 6 Comparison of computed and measured fin surface pressures on the cranked tail configuration at $\alpha = 7.8$ deg.

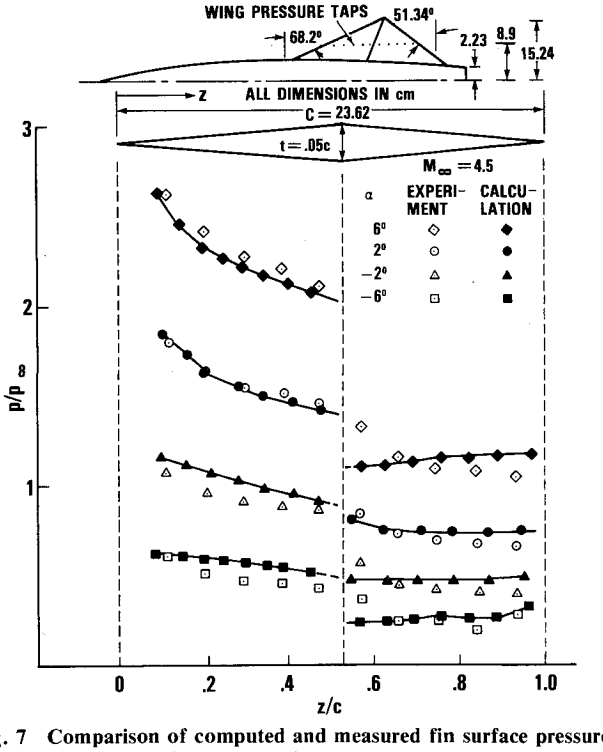

Fig. 7 Comparison of computed and measured fin surface pressure as a function of incidence at Mach 4.5.

A comparison of measured and calculated fin surface pressure distributions for the clipped delta wing at an incidence of 3.8 deg is provided in Fig. 4 where the leeward and horizontal fin surfaces are shown. Comparison of the calculated and measured fin surface pressures on the cranked tail are shown in Figs. 5 and 6 for incidences of 3.8 and 7.8 deg.

A detailed examination of Figs. 4-6 indicates that good agreement is obtained in most cases between measured and calculated fin surface pressures. The scatter in the experimental data is a result of plotting experimental measurements from several different runs. The calculated

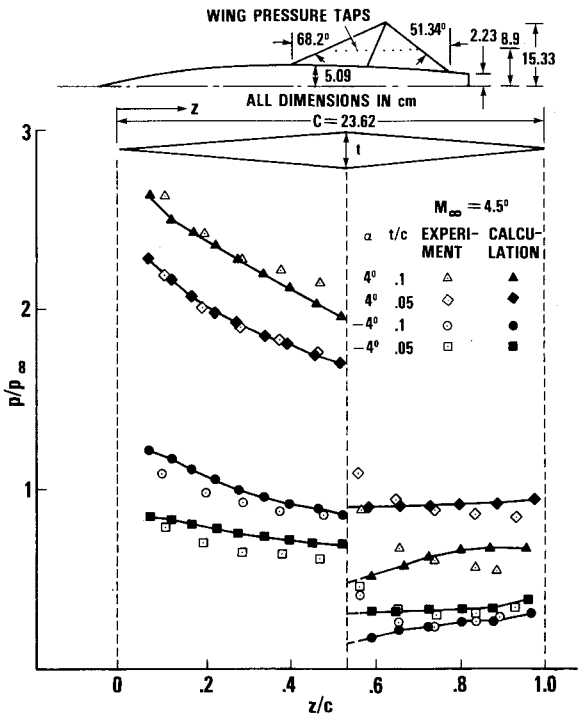

Fig. 8 Comparison of computed and measured fin surface pressures on wings of varying thickness at $\alpha = \pm 4$ deg and Mach 4.5.

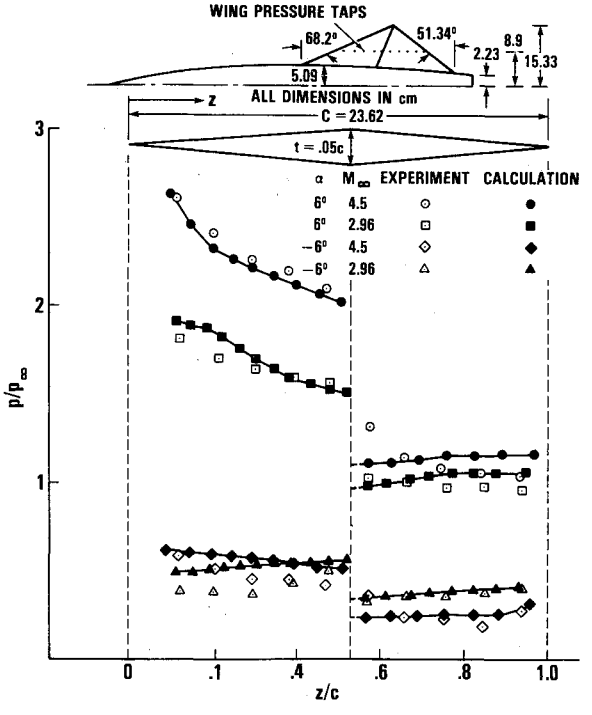

Fig. 9 Comparison of computed and measured fin surface pressures at varying Mach numbers at $\alpha = \pm 6$ deg.

pressure exhibits abrupt jumps at surface slope discontinuities while experimental values show a more gradual transition. This is to be expected since shock or expansion discontinuities are introduced at such points in the numerical procedure that neglect the smoothing influence of viscosity. On fin surfaces which feature strong leading-edge shocks, poor agreement is obtained along the root chord. The leading-edge pressure is overpredicted and the calculated pressure jumps occurring at the various surface discontinuities also tend to be greater than experimental values. The interaction of the thick corner boundary layer and the leading-edge shock presumably have a large influence on the corner and accounts for much of this discrepancy. Another area of disagreement occurs along the tip. Here predicted and measured pressures are of similar value, but the experimental pressure profile features a negative slope while the numerical pressure distribution is almost constant. It is not clear whether this discrepancy is due to viscous phenomena. On fin surfaces that have a weak leading-edge shock or expansion, the predicted and measured fin tip pressure profiles are in good agreement. Also, the leading-edge pressure at the corner is close to the experimental value. Over the entire span, calculated pressures on the trailing-edge panel tend to be less than measured, probably reflecting the existence of a very thick boundary layer or separation.

Wind tunnel tests on the swept wing configurations of Ref. 15 (see Fig. 7) offer an opportunity to compare calculation with experiment for cases where detached shock waves are predicted to occur. As was indicated in Sec. III, the upper and lower wing surfaces are treated independently and a detached shock affects only the generating compressive surface. Numerical experiments on the compressive wing surface for this type of configuration indicate that both the correct pressure level and streamline direction must be assigned at the leading edge. The prescribed leading-edge pressure value controls the pressure level near the leading edge while the streamline direction influences its value farther downstream.[11] As the assigned streamline direction is turned away from the body, the pressure far from the leading edge decreases. A comparison of experiment and calculation suggests the following simple algorithm for determining streamline direction. The angle $\beta_0 = \tan^{-1}(u/w)$ is determined prior to adjusting the flow for the presence of the leading edge. The final streamline direction is set to insure that $u/w = \tan(2.5\beta_0)$. Based on an examination of the experimental data of Ref. 15, an algorithm has been determined empirically for assigning surface pressure values. The flow is considered to pass through an oblique shock which makes an angle σ_s with the velocity vector in the plane normal to the leading edge. The value of σ_s is determined from: $\sigma_s = 90$ deg $-(90$ deg $-\delta^*)\lambda$ where $\lambda = \{1.48$ for $\delta/\delta^* < 1.13$, $2.36 - 0.8(\delta/\delta^*)$ for $1.13 \le \delta/\delta^* < 2.17$, $-17.0 + 16.41\,(\delta/\delta^*) - 3.82\,(\delta/\delta^*)^2$ for $2.17 \le (\delta/\delta^*) < 2.55$ and 0.00 for $(\delta/\delta^*) \ge 2.55\}$. Here δ^* is the maximum possible turning angle with an attached shock, and δ is the turning angle of the component normal to the leading edge. If the angle σ is equal to 90 deg the Mach number of the leading-edge normal component downstream of the shock is reduced from M_f^* to M_f using the expression

$$M_f = [1 - 0.057\chi + 0.22 \sin(\pi\chi/17.5)]M_f^*$$

where

$$\chi = (\delta - 2.55\delta^*)(1 - M_f^*)^{0.25}$$

The equations just given predict the leading-edge pressure fairly accurately on compressive surfaces featuring detached shocks for the tested swept wing configuration over a Mach number range of 2.96-4.5.

Calculations have been compared to experiment for the thick and thin wing configurations of Ref. 15 at the Mach numbers of 2.96, 3.95, and 4.5, and at angles of attack of 0, ± 2, ± 4, and ± 6 deg. The measurements were taken at a Reynolds number of 5×10^5 based on the body diameter and freestream conditions. (Here positive and negative incidence refers to the compression and expansion wing surfaces, respectively.) The configuration geometry, which features wing surface slope discontinuities, and sample results are shown in Figs. 7-9. These graphs indicate that the current computations accurately reflect changes in Mach number, angle of attack, and wing thickness. The present numerical procedure does not attempt to account for boundary-layer effects, and the predicted pressure jumps at the wing slope discontinuities are abrupt in contrast to experimental

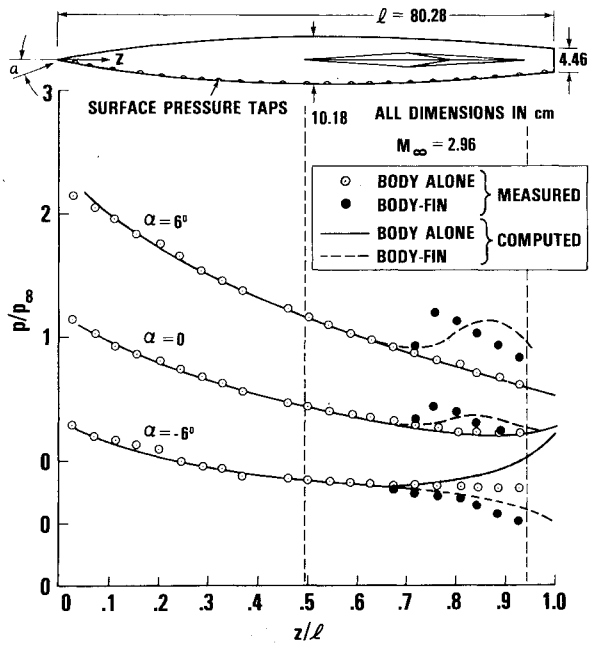

Fig. 10 Calculated and measured body surface pressures with and without fins on the windward and leeward meridian at Mach 2.96.

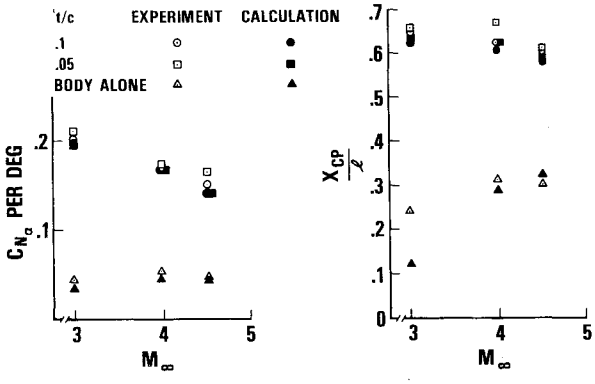

Fig. 11 Comparison of calculated and measured normal force and center of pressure as a function of Mach number for body alone, thin fin, and thick fin configurations.

measurements. A detailed examination of Figs. 7-9 indicates that best results are obtained on the compressive surfaces at the higher Mach numbers. On the expansion wing surfaces at the higher incidences, the leading-edge pressure prediction provided by the Prandtl-Meyer expansion is often larger than experimental values. This may be due to the presence of a thick boundary layer.

The data of Ref. 15 also include pressure measurements along a pitch plane body meridian. At positive incidences the instrumented ray is on the windward side of the body while at negative incidences it is on the lee side. These measurements are compared to numerical results at an incidence of 6, 0, and -6 deg in Fig. 10 for a Mach number of 2.96. At $\alpha = 6$ deg the body alone data are in good agreement with experiment, and the influence of the wing on the body causes an increase in the experimentally measured pressure. This increase is correctly reflected by the calculations, but the peak predicted values are located approximately one caliber downstream of the measured ones. At an incidence of 0 deg, the same trend is visible but the lagging appears to be somewhat less. When the angle of attack is changed to -6 deg, the presence of the wing causes a decrease in body pressure. In this case the body alone calculation does not agree well with experiment, presumably due to viscous effects. The body features a decreasing diameter near the base which undoubtedly results in changes in the effective body shape due to boundary layer thickening or separation. The calculated flowfield features a crossflow shock near the base that produces an increase in the leeward meridian pressure profile. The numerical results for the body-wing configuration are much closer to experiment and feature the correct downward change in the body surface pressure. The predicted onset of the wing influence on the leeward meridian body pressure does not appear to lag the experimentally measured one.

Several factors may contribute to the lag in the predicted wing influence on windward body surface pressure. The body boundary conditions are not in conservation form and the calculated shock speed may be inaccurate. The thin fin assumption places the wing surface at the chord position which increases the distance to the windward meridian and may delay the arrival of the wing leading-edge shock. The subsonic region within the boundary layer may transmit the influence of the wing at a greater rate than does the supersonic, inviscid outer flow. The fact that a lag in leading-edge expansion transmission is not detectable suggests that the principal cause of this problem is inaccuracies in tracking the leading-edge shock along the body surfaces.

A comparison of predicted and measured normal force and center of pressure for the body alone and the fin-body configurations is shown in Fig. 11. In the body alone case, relatively good agreement is obtained at $\alpha = 2$ deg for Mach numbers of 3.95 and 4.5. At Mach 2.96 there is a large discrepancy between experiment and computation, particularly with respect to center of pressure. An examination of the leeward pressure profiles indicates that the calculation features a weak crossflow shock near the body base while experimental pressure profiles smoothly decrease. The difference is most likely due to lee side viscous effects. The presence of the fin suppresses the crossflow shock formation producing better agreement between calculation and experiment.

V. Concluding Remarks

A numerical method has been developed that predicts the inviscid supersonic flowfield about finned configurations of engineering interest. The computational requirements are by design modest; for example, the wing-body and cruciform body-tail cases examined in the preceding sections nominally required 3 and 7 min, respectively, of CPU time on a CDC 6500. The current study differs from previous work by treating the fin and body geometries separately. At present, a thin fin approximation is employed that limits the applicability of the computational procedure to relatively slender fins with sharp leading edges. The fins must approximately lie along planes that intersect at a line inside the missile body. With this formulation it is possible to treat a wide variety of configurations of engineering interest that can feature an arbitrary number of fins and tails with small deflection, camber, or variation in dihedral. The presented results suggest that the current approach predicts adequately inviscid flowfields over finned bodies featuring supersonic fin edges using meshes that are sufficiently coarse to allow rapid engineering calculations.

Acknowledgments

This work was jointly supported by the Naval Sea Systems Command and the Naval Air Systems Command. The authors would also like to acknowledge the enthusiastic support of Frank Moore of the Naval Surface Weapons Center, Dahlgren, Va., throughout the course of this investigation.

References

[1] Thomas, P. D., Vinokur, M., Bastianon, R., and Conti, R. J., "Numerical Solution for Three-Dimensional Inviscid Supersonic Flow," *AIAA Journal*, Vol. 10, July 1972, pp. 887-894.

[2]Moretti, G., Grossman, B., and Marconi, F., "A Complete Numerical Technique for the Calculation of Three-Dimensional Inviscid Supersonic Flows," AIAA Paper 72-192, San Diego, Calif., 1972.

[3]Marconi, F. and Salas, M., "Computation of Three Dimensional Flows about Aircraft Configurations," *Computers and Fluids*, Vol. 1, June 1973, pp. 185-195.

[4]Kutler, P., Reinhardt, W. A., and Warming, R. F., "Multishocked, Three-Dimensional Supersonic Flowfields with Real Gas Effects," *AIAA Journal*, Vol. 11, May 1973, pp. 657-664.

[5]Kyriss, C. L. and Harris, T. B., "A Three-Dimensional Flow Field Computer Program for Maneuvering and Ballistic Re-entry Vehicles," Tenth United States Navy Symposium on Aeroballistics, July 1975.

[6]Marconi, F., Salas, M., and Yaeger, L., "Development of a Computer Code for Calculating the Steady Super/Hypersonic Inviscid Flow Around Real Configurations, Vol. I-Computational Techniques," NASA CR 2675, April 1976.

[7]Solomon, J. M., Ciment, M., Ferguson, R. E., and Bell, J. B., "Inviscid Flowfield Calculations for Reentry Vehicles with Control Surfaces," *AIAA Journal*, Vol. 15, Dec. 1977, pp. 1742-1749.

[8]Moretti, G., "Conformal Mappings for Computation of Steady, Three-Dimensional, Supersonic Flows," *Numerical/Laboratory Computer Methods in Fluid Dynamics*, ASME, Vol. 13, 1976.

[9]Hindman, R. S., Kutler, P., and Anderson, D., "A Two-Dimensional Unsteady Euler-Equation Solver for Flow Regions with Arbitrary Boundaries," AIAA Paper 79-1465, Williamsburg, Va., 1979.

[10]Solomon, J. M., Ciment, M., Ferguson, R. E., Bell, J. B., and Wardlaw, A. B., "A Program for Computing Steady Inviscid Three-Dimensional Supersonic Flow on Reentry Vehicles, Vol. 1: Analysis and Programming," Naval Surface Weapons Center/White Oak, Silver Spring, Md., NSWC/WOL TR 77-28, Feb. 1977.

[11]Wardlaw, A. B., Solomon, J. M., and Baltakis, F. P., "Supersonic Inviscid Flowfield Computations of Missile Type Bodies," AIAA Paper 80-0271, Pasadena, Calif., Jan. 1980.

[12]Landau, L. D. and Lifshitz, E. M., *Fluid Mechanics*, Pergamon Press (Addison-Wesley), 1959.

[13]Ferri, A., "Supersonic Flows with Shock Waves," *General Theory of High Speed Aerodynamics and Jet Propulsion*, Vol. 7, edited by W. R. Sears, Princeton University Press, 1954.

[14]Lamb, M., Sawyer, W. C., Wassum, D. L., and Babb, C. D., "Pressure Distributions on Three Different Cruciform Aft-Tail Control Surfaces of a Wingless Missile at Mach 1.60, 2.36 and 3.70," Vols. II and III, NASA TM 80097, Aug. 1979.

[15]Jackson, C. M. Jr. and Sawyer, W. C., "A Method for Calculating the Aerodynamic Loading on Wing-Body Combinations at Small Angles of Attack in Supersonic Flow," NASA TN D-6441, 1971.

From the AIAA Progress in Astronautics and Aeronautics Series

SPACECRAFT CHARGING BY MAGNETOSPHERIC PLASMAS—v. 47

Edited by Alan Rosen, TRW, Inc.

Spacecraft charging by magnetospheric plasma is a recently identified space hazard that can virtually destroy a spacecraft in Earth orbit or a space probe in extra terrestrial flight by leading to sudden high-current electrical discharges during flight. The most prominent physical consequences of such pulse discharges are electromagnetic induction currents in various on-board circuit elements and resulting malfunctions of some of them; other consequences include actual material degradation of components, reducing their effectiveness or making them inoperative.

The problem of eliminating this type of hazard has prompted the development of a specialized field of research into the possible interactions between a spacecraft and the charged planetary and interplanetary mediums through which its path takes it. Involved are the physics of the ionized space medium, the processes that lead to potential build-up on the spacecraft, the various mechanisms of charge leakage that work to reduce the build-up, and some complex electronic mechanisms in conductors and insulators, and particularly at surfaces exposed to vacuum and to radiation.

As a result, the research that started several years ago with the immediate engineering goal of eliminating arcing caused by flight through the charged plasma around Earth has led to a much deeper study of the physics of the planetary plasma, the nature of electromagnetic interaction, and the electronic processes in currents flowing through various solid media. The results of this research have a bearing, therefore, on diverse fields of physics and astrophysics, as well as on the engineering design of spacecraft.

304 pp., 6 x 9, illus. $16.00 Mem. $28.00 List

TO ORDER WRITE: Publications Dept., AIAA, 1290 Avenue of the Americas, New York, N. Y. 10019